Short and medium range structures of 80GeSe2-20Ga2Se3 chalcogenide glasses

Elena Petracovschi, Laurent Calvez, Laurent Cormier, David Le Coq, Jincheng Du

Short and medium range structures of $80GeSe_2$-$20Ga_2Se_3$ chalcogenide glasses

Elena Petracovschi[a, c], Laurent Calvez[a], Laurent Cormier[b], David Le Coq[a], Jincheng Du[c,*]

[a]*Univ Rennes, CNRS, ISCR (Institut des Sciences Chimiques de Rennes)-UMR6226, F-35000 Rennes, France*

[b]*Sorbonne Université, CNRS, MNHM, IRD, Institut de Minéralogie de Physique des Matériaux et de Cosmochimie, F-75005 Paris, France*

[c]*University of North Texas, Department of Materials Science and Engineering, Denton, TX 76203, United States*

([*]Corresponding author. email: du@unt.edu)

Abstract

The short and medium range structures of the $80GeSe_2$-$20Ga_2Se_3$ (or $Ge_{23.5}Ga_{11.8}Se_{64.7}$) chalcogenide glasses have been studied by combining *ab initio* molecular dynamics (AIMD) simulations and experimental neutron diffraction studies. Structure factor and total correlation function were calculated from glass structures generated from AIMD simulations and compared with neutron diffraction experiments showing reasonable agreement. The atom structures of the ternary chalcogenide glasses were analyzed in detailed and it was found that gallium atoms are four-fold coordinated by selenium and form [$GaSe_4$] tetrahedra. Germanium atoms on average also have around four-fold coordination, among which 3.5 is selenium with the remaining being Ge-Ge homo-nuclear bonds. Ga and Ge tetrahedra link together through mainly corner-sharing and some edge-sharing. No homo-nuclear bonds were observed among Ga atoms or between Ge and Ga. In addition, selenium-selenium homo-nuclear bonds were observed and form Se chains with various lengths. A small fraction of selenium atom triclusters that bond to three cations of Ge and Ga were also observed, confirming earlier proposals from Se solid state NMR studies. Furthermore, electronic structure of the ternary chalcogenide glasses were studied in terms of atomic charge, chemical bonding and electronic density to gain insights on the chemical bonding in the glass and electronic properties and to provide explanation of observed atomic structures.

Key words: AIMD, chalcogenide glasses, Ga-Ge-Se, glass structure, electronic property

1. Introduction

Chalcogenide glasses refer to a type of inorganic glasses that contain at least one type of main group VI chalcogenide elements (such as S, Se, or Te) except oxygen. Chalcogenide glasses have a number of unique optical and optoelectronic properties, such as high refractive and high optical non-linearity, low phonon energy, high optical transparency in the infrared region, high photoconductivity and laser induced conductivity changes due to phase transition [1,2]. Because of these intriguing physical properties, they find applications in infrared optics, memory, optoelectronics, infrared sensing and other fields. One of the most important properties of these glasses is their high transparency in the infrared range. Their transparency in the two atmospheric windows (3-5 μm) and (8-12 μm) leads to applications as infrared optics such as lenses for IR cameras and sensors in the infrared range [3–5]. As compared to other infrared transmission materials such as single crystal germanium or polycrystalline ZnS or ZnSe, chalcogenide glasses have notable advantages due to their easier synthesis and forming processes and the ability to form in large and complex shapes [6]. Chalcogenide glass-ceramics have been extensively studied due to their improved mechanical properties such as high modulus of flexural strength, hardness or toughness, achieved by introducing crystalline phases in the glassy matrix [7–15]. The crystallization step, nevertheless, needs to be carefully controlled and the glass composition well designed to enable precipitation of targeted phases in order to obtain uniform size and homogenous distribution of crystals to preserve the optical transmission of the base glass. Detailed information of the glass structure is highly valuable to understand the above-mentioned physical properties and crystallization processes. The purpose of this work is to combine *ab initio* molecular dynamics (AIMD) simulations and experimental diffraction studies to understand the structural features of ternary GeGaSe chalcogenide glass that has the capability to form both homogeneous glass and glass-ceramics through post heating treatment.

The structure of chalcogenide glasses is very different and usually more complicated than the conventional oxide glasses [1, 2]. This is mainly due to the differences in their chemical bonding: in chalcogenide glasses there exist mixed covalent, ionic and even some metallic bonding characteristics while in oxide glasses there are mainly ionic bonding with some covalent

characters. As a result, the cations in oxide glasses are coordinated by oxygen anions and cation-cation direct bonding is avoided to prevent high energy states. In chalcogenide glasses, however, there exist homo-nuclear bonds, such as metal - metal or non-metal - non-metal bonds, and, for some structures, there exist of molecular type structural groups. The nature of these mixed chemical bonding leads to more complicated structure characteristics that pose challenges in both simulation and experimental characterizations. On the other hand, chalcogenide and oxide glasses do share some structural similarities. For example, the Ga_2Se_3-$GeSe_2$ glasses are frequently compared to Al_2O_3-SiO_2 glasses, where SiO_2 and $GeSe_2$ are considered as glass former while Al_2O_3 and Ga_2Se_3 are classified as intermediates, despite the above mentioned bonding and structural differences between the two types of glasses.

The pseudo binary Ga_2Se_3-$GeSe_2$ (or ternary Ga-Ge-Se) chalcogenide glasses have been extensively studied and shown promising physical properties [16, 17]. Their structures have also been studied by several characterization techniques and significant structure insights were obtained for these glasses. For example, Mao et al. studied the structure of Ga_2Se_3-$GeSe_2$ glasses with up to 30 mol% of Ga_2Se_3 by using Raman and multinuclear NMR (^{71}Ga and ^{77}Se) [17]. The results show that the glass structure is mainly made of corner sharing [Ge/$GaSe_4$] tetrahedra but with some fraction of edge sharing [$GeSe_4$] units. With increasing of Ga_2Se_3, Ge-Ge homonuclear bonds were formed to satisfy the four-fold coordination requirement of both Ga and Ge. At high Ga_2Se_3 concentration, triply coordinated Se was formed due to Se deficiency and the structural requirements to form cation four-fold coordination. In another study using ^{77}Se MATPASS/CPMG NMR, Mao et al. studied the effect of selenium deficiency on the glass structure and found that at with Ga_2Se_3 concentration being higher than 30%, three-coordinated Se was formed as another mechanism to accommodate Se deficiency in addition to the formation of ($Se_{3/2}$)Ge-Ge($Se_{3/2}$) ethane like homo-nuclear bonds [18]. Golovchak et al. studied the effect of Ga addition on the structure of Ge-Se glasses by using XPS and EXAFS [19]. It was found that both Ga and Ge are mostly four-fold coordinated, consistent with NMR studies. Addition of Ga was found to facilitate more uniform distribution of Se as compared that in the GeSe glasses. It was suggested that 4-fold coordinated Ga, rather than 4-fold coordinated Ge, were preferentially formed in the Ga-Ge-Se glass. Ge satisfies its four-fold coordination by forming homonuclear

Ge-Ge bonds or Ge-Ga bonds. Additionally, the authors suggested no evidence of 3-fold coordinated Se atoms [19]. In a recent study, Petracovschi et al. have studied the structures of $GeSe_4$ and $80GeSe_2$-$20Ga_2Se_3$ glasses obtained from mechanical milling by using ^{77}Se NMR and Raman spectroscopy [16]. A small amount of edge-sharing [$GeSe_4$] tetrahedra were observed in selenium rich $GeSe_4$ glass but not in the ternary system. It was shown that there exist Se-Se homonuclear bonds and selenium chain structures. In another study, the short-range structure of Ge-Ga-Se glasses were studied using EXAFS with Ge, Ga, and Se absorption K-edges [20]. The EXAFS data were interpreted by using Reverse Monte Carlo modeling [20]. It was found both Ge and Ga are four-fold coordinated. Surprisingly, the authors found that the fitting quality can be improved by introducing Ga-Ge bonds and concluded that Ga enters the glass network through Ga-Ge bonding. It was argued that the formation of Ga-Ge bonds can free Se from Ge to form Se-Se bonds. However, this was not supported by other experimental studies. Hence these experimental investigations gained insights on the structure of the Ga-Ge-Se chalcogenide glasses but there are still several unanswered questions of the complex structures, e.g. the formation of Ga-Ge bonds and Se triclusters.

Computer simulations, mostly first principles based, have been employed to obtain short and medium range structural information of chalcogenide glasses. There are attempts to develop empirical potentials for simple chalcogenide glass systems from accurate first principles calculations [21, 22], the structure and bonding complexity, as mentioned earlier, make this a daunting task. *ab initio* molecular dynamics simulations in the frameworks of Car-Parrinello or Born-Oppenheimer [23] have been applied to the study of oxide [24, 25] and chalcogenide glasses [26, 28]. A number of AIMD simulations of binary chalcogenide glasses such as $GeSe_2$ or $GeSe_4$ [26, 28-30] have been performed and considerable structural insights of these glasses have been obtained from these simulations alone or in combination with experimental studies [27, 29]. However, fewer simulation studies concerning ternary chalcogenide glasses were reported [31] and those reported were focused on Ge-Sb-Te phase change chalcogenide systems [32-34].

In this paper, we investigated the structure of the ternary Ge-Ga-Se glasses with composition $Ge_{23.5}Ga_{11.8}Se_{64.7}$ ($80GeSe_2$-$20Ga_2Se_3$), by combining experimental neutron

diffraction data and *ab initio* molecular dynamics simulations. The reason to choose this glass composition is due to its importance as a model system for chalcogenide glass and glass-ceramics. Importantly, the structure of these glasses has been extensively studied in experiments [13-18], which can also be used to compare with the simulation data. From the comparison of the experimental and AIMD results, structural insights on the short range bonding environments were gained from the detailed atomistic models. Based on these structural models, information on electronic structures were also obtained.

2. Experimental and simulation methodology

2.1 Glass synthesis and characterizations

The pure raw starting elements, germanium (5N, Umicore), gallium (6N, Cerac), and selenium (5 N, Umicore) were introduced in a silica tube (10mm diameter) and pumped under vacuum (10^{-6} Pa) for several hours before being sealed. The ampoule was then placed into a rocking furnace and heated up to 900°C for 12 hours and finally quenched in water to obtain a bulk glass.

The quenching induces stress within the glass. Thus, in order to relax these constraints, the glass was annealed at 10°C below Tg. After annealing, the silica ampoule was cautiously broken to remove the bulk chalcogenide glass.

The characteristic temperatures of the glass were obtained by thermal analysis DSC (Q20 TA Instruments) on a sample of 10 mg with a heating ramp of 10°C/ min. The X-ray diffractograms were recorded for four hours using a Philips PW3020 diffractometer with Cu Kα line and a measurement step of 0.02°.

2.2 Neutron diffraction experiment details

Neutron diffraction experiments were carried out at the 7C2 diffractometer (LLB, Saclay) [40]. The wavelength of the incident radiation was λ=0.724 Å. Powdered samples were filled into vanadium cans with 7 mm diameter and 0.1 mm wall thickness. The neutron beam height was fixed at 5 cm. Diffraction data were collected at room temperature for 10 hours approximately The neutron structure factors $S_N(Q)$ was obtained from the scattered intensities

after conventional data reduction was applied for absorption, incoherent and multiple scattering. Inelastic effects were treated by a Placzek type correction.

The total pair correlation functions $g(r)$ of neutron experiments were obtained by a Fourier transformation of $S_N(Q)$ as follows:

$$g(r) = 1 + \frac{1}{2\pi\rho_0 r}\int (S_N(Q) - 1)Qsin(Qr)dQ \qquad (1)$$

where ρ is the average number density of the samples. The corresponding total correlation functions $T(r)$ were then calculated following the equation (2):

$$T(r) = 4\pi r\rho_0 g(r) \qquad (2)$$

2.3 AIMD simulations of $80GeSe_2$-$20Ga_2Se_3$ glasses

Molecular dynamic simulations were performed by using plane wave density function theory (DFT) using the Vienna *ab initio* Simulation Package (VASP). The exchange and correlation energies were described using generalized gradient approximation (GGA) functional with the Perdew-Burke-Ernzerhof (PBE) parameterization [35]. It has been shown the choice of functional plays an important role in the final glass structures for chalcogenide glasses [26]. The GGA PBE functional was chose due to its capability to describe the structure and properties of gallium selenide (Ga_2Se_3) and germanium selenide ($GeSe_2$) polymorphs based on the calculation of the equation of states of these crystalline phases. For the crystalline phase calculations, Monkhorst Pack K-space meshing was used with $0.3Å^{-1}$ spacing and a single Γ point sampling was used for glass systems. The kinetic energy cutoff for plane waves was 400 eV, which was determined by convergence testing with total energy of the crystalline systems. These results suggest that the adopted DFT functional is capable to describe the ternary Ga-Ge-Se system.

The glass structures were generated using Born-Oppenheimer AIMD [23] in which at each of the ionic step, electronic ground states were obtained based on plane wave DFT calculations, from which the forces acting on each atom were calculated to drive the move of atoms in the next step. Three initial structures were randomly generated with minimum distance cutoffs of the atom pairs to avoid initial unphysical atom positions. Due to high computational cost of the AIMD

simulations, the chosen simulation cell contains 170 atoms in the cubic shape with a length of 17.12 Å for each side, which corresponds to the experimental density of 4.3 g/cm^3. After initial geometry optimization, the glasses were generated using a melt-quenching process with a time step of 1 fs. The Nosé's thermostat were used to control the temperature [36]. After an initial relaxation at zero K, the configurations were heated up to 3000 K for 20 ps to obtain the melt structure. Then, the melts were gradually cooled down, to 2000 K, 1000 K and 300 K. At each temperature, the system was maintained during 20 ps, which leads to a nominal cooling rate of 150K/ps. Three glasses were made from different initial atomic positions and the statistics of structures were averaged among the three glasses at room temperature.

2.4 Structural analysis of the simulated glass

The local structure of the $80GeSe_2$-$20Ga_2Se_3$ glass has been analyzed by calculating the pair correlation functions, Ge and Ga coordination number distributions, and bond angle distributions (BAD). The coordination numbers were determined using cutoff distances determined from the first minimum distances of the corresponding partial pair correlation functions and are: 2.50 Å for Ge–Se and 2.44 Å for Ga–Se.

In order to compare with the experimental neutron structure factor and the total correlation functions, the partial pair correlation functions $t_{ij}(r)$ were first broadened by convoluting with the component peak function $p_{ij}^{N}(r)$, which is defined by the experimental resolution due to a Q-range limited to a Q_{max} value, the maximum value of the experimental scattering vector.

$$t'_{ij}(r) = \int_0^\infty t_{ij}(r')[P_{ij}^N(r-r') - P_{ij}^N(r+r')]dr' \qquad (3)$$

The component peak function is defined as,

$$P_{ij}^N(r-r') = \frac{\overline{b_i}\cdot\overline{b_j}}{\pi}\int_0^{Q_{max}} M(Q)\cos(rQ)\,dQ \qquad (4)$$

in which $\overline{b_i}$ is the average neutron scattering length of atom i, Q_{max} is as defined earlier, $M(Q)$ is the modification function. A common form of modification function is the Lorch function, which gives a gradual cutoff and is defined as,

$$M(Q) = \begin{cases} \frac{sin\Delta r}{\Delta rQ} & Q \le Q_{max} \\ 0 & Q > Q_{max} \end{cases} \quad (5)$$

The total correlation function after broadening for the neutron diffraction case is then expressed as,

$$T^N(r) = T^0(r) + D^N(r) = \sum_{ij} c_i(t_{ij}) \quad (6)$$

in which $T^o(r)$ equals $4\pi r\rho_0 \sum_i c_i \bar{b_\iota}$, where c_i and $\bar{b_\iota}$ are atom fraction and neutron scatter length of element *i*, ρ_0 is the atom number density of the glass.

To compare in reciprocal space, the partial structure factors are first obtained through Fourier transformation of the partial pair distribution functions using

$$S_{ij}(Q) = 1 + \rho_0 \int_0^R 4\pi r^2 [g_{ij}(r) - 1] \frac{\sin(Qr)}{Qr} \frac{\sin(\frac{\pi r}{R})}{\pi r/R} dr \quad (7)$$

in which $g_{ij}(r)$ is the pair distribution function of atomic *i-j* pair, R is the maximum value of the integration in real space which is set to half of the size of one side of the simulation cell . The $\frac{\sin(\frac{\pi r}{R})}{\pi r/R}$ part of the integrand is a Lorch-type window function, as defined earlier, to reduce the effect of finite simulation cell size. Lorch function reduces spurious oscillations at low Q (the cutoff effect) but it can also lead to some broadening of the peaks. It is valuable to study the cutoff effect by simulating several glasses with different simulation cell sizes as shown in earlier simulations [42] but this was not performed in this work due to high computational cost of AIMD simulations. The partial structure factors are then added together with weighting factors to obtain the total neutron structure factor:

$$S_N(Q) = \left(\sum_{i=1}^n c_i \bar{b_\iota}\right)^{-2} \sum_{i,j=1}^n c_i c_j b_i\, b_j S_{ij}(Q) \quad (8)$$

2.5 Electronic structure and bonding analysis

Electronic density of states was calculated from the fully relaxed final configurations of the glasses at 300K. Bader atomic charge analyses were performed based on these structures to obtain bonding information of these glasses. Electronic Density of States (EDOS) of the glasses were calculated and partial elemental contribution determined.

3. Results and Discussions

3.1 Experimental results of structure determination from neutron diffraction

As shown in Figure 1 (a), X-ray diffraction pattern demonstrate the full amorphization of the $80GeSe_2$-$20Ga_2Se_3$. The experimental structure factor obtained in neutron diffraction depicted in Figure 1 (b) further supports the amorphous nature of these glasses. This is of great importance as this glass composition present a strong tendency to crystalize when made by the conventional melt and quench technique. This is manifested by the thermal analyses of these glasses reported later. Careful sample preparation ensured the amorphous nature of these glasses that make high quality comparison with simulations possible. Thermal analysis showed the glass transition temperature (Tg) was 358°C and the crystallization temperature (Tx) being 448°C with a ΔT (Tx-Tg) less than 100°C, which suggests that the glass is a relatively unstable glass and, consequently, a good system for glass-ceramic formation.

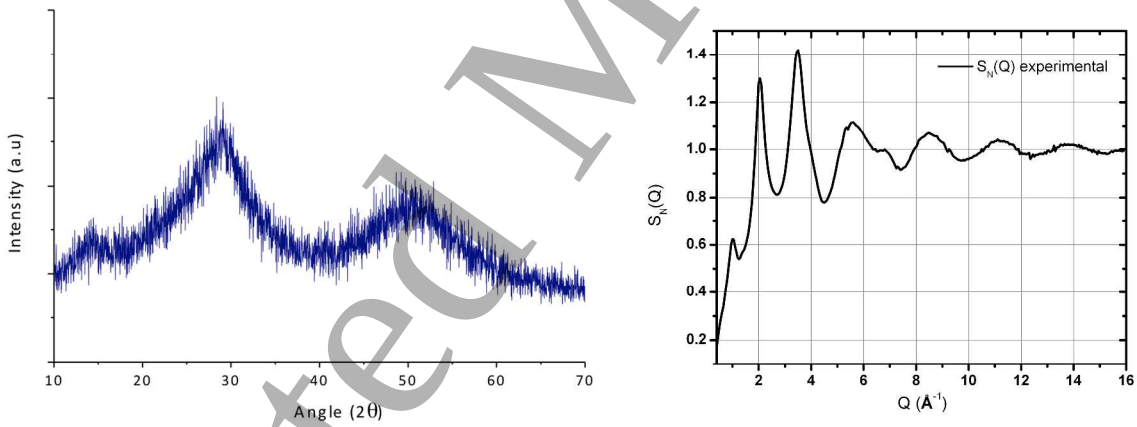

Fig. 1. (a) X-ray diffraction pattern and (b) neutron structure factor demonstrate fully amorphous nature of the $80GeSe_2$-$20Ga_2Se_3$ glass.

3.2 Comparison of experimental and simulated structure features

Comparison of the simulated and experimental neutron structure factors and total correlation functions are shown in Fig. 2 (a) and (b) respectively. For neutron structure factor, the peak positions are in general good agreement but the first peak from simulation is broader and shifted slightly to higher Q values, while the 2nd and 3rd peaks are in good agreement with experiments. The difference of the first peak is partly due to peak broadening during the Fourier transformation from real space partial pair distribution functions due to the relatively small simulation box used in the AIMD simulations. The real space total correlation function from simulations and experiments are compared in Fig. 2(b), which showed general agreement. The first peak and second peak position and relative intensity are in reasonable agreement between simulations and experiments, while the first peak from simulations slight shifted to a higher r value by 0.2 Å. The R_x factor that measures the quality of agreement between experimental and simulations [44] was calculated from 1-8 Angstrom for real space total correlation function T(r) (Fig. 2(b)) and found to be 9.9%. This shows the agreement between the simulated structure and experiments is reasonable although not perfect. As shown later in the deconvoluted partial pair correlation functions (Fig. 4), the first peak is mainly due to the Ge-Se, Se-Se and Ga-Se contributions. The second peak is mainly due to Se-Se second peak contribution. More detailed assignments of the peak contributions are shown in the next section. Despite discrepancies between experiment and simulations partially due to small simulation sizes in AIMD simulations, the reasonable agreements in both reciprocal and real space comparison suggests that the general structure features of the chalcogenide glasses were reproduced in the models from AIMD simulations.

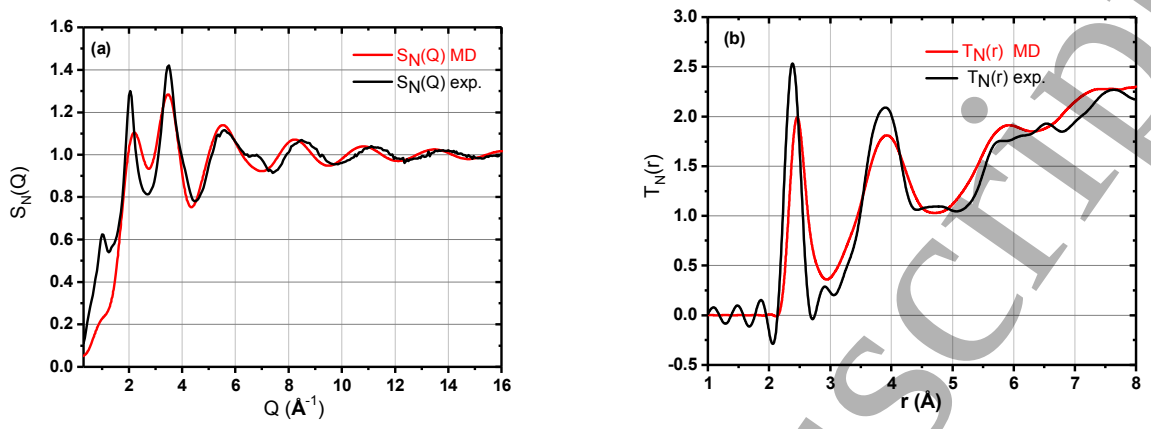

Fig. 2. Comparison between experimental (red line) and calculated neutron data (black line) in the reciprocal and real spaces for the $80GeSe_2$-$20Ga_2Se_3$ glass: (a) the structure factors $S_N(Q)$ in the 0.5-16 $Å^{-1}$ Q-range and (b) the total correlation functions $T_N(r)$ in the 1-8 Å r-range.

3.3 General structural features of GeGaSe glasses from AIMD simulations

The snapshot of the configuration of $80GeSe_2$-$20Ga_2Se_3$ glasses from AIMD simulations is shown in Fig. 3 (a). The represented local arrangements showing a long Se-Se chain and surrounding [$GeSe_x$] and [$GaSe_4$] polyhedrons are shown in Fig. 3 (b). It can be seen that $GaSe_4$ and $GeSe_4$ tetrahedra are the main structural motifs in the glass. Importantly, structure features such as Se-Se bonds and Se chains, as well as Ge–Ge homo-nuclear bond are both observed. Se chains have been observed experimentally in the $80GeSe_2$-$20Ga_2Se_3$ glass using ^{77}Se solid state NMR and in other Se-rich glasses such as $GeSe_x$ (x = 4, 6, 8), $AsSe_y$ (y = 3, 4.5, 9) and $TeSe_z$ (z = 1, 2, 3, 4, 9) [37–39]. Ge-Ge homonuclear bonds were also suggested from NMR and XPS studies in the ternary Ga-Ge-Se glasses. These structural features thus agree well with the experimentally derived structural models of these glasses. Atomistic simulations, however, provide much more detailed structure information that will be analyzed below.

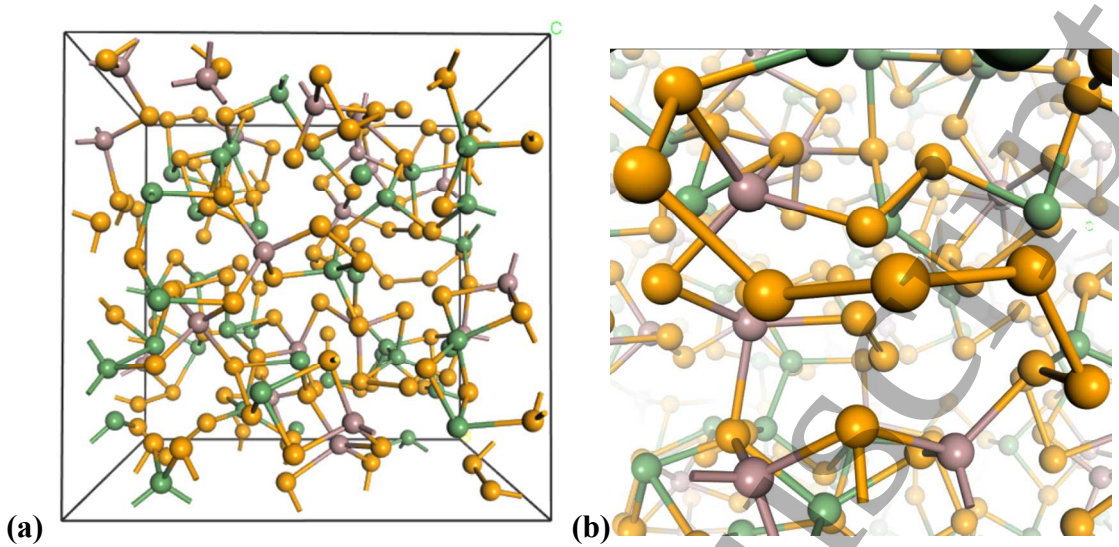

Figure 3: Snapshot of the total simulation cell (a) and (b) zoomed in structure showing a long Se-Se chain and Ge/Ge-Se tetrahedral in the background of the $80GeSe_2$-$20Ga_2Se_3$ glass (yellow balls: Se; green balls: Ge; purple balls: Ga) from AIMD simulations.

Fig. 4 (a) shows the calculated neutron diffraction total and partial correlation functions in $80GeSe_2$-$20Ga_2Se_3$ glasses. The peak around 2.5 Å is mainly due to Se–Ge and Se–Ga pairs but it contains also a non-negligible Se–Se contribution which suggests that a considerable amount of homo-nuclear Se–Se bonds can be observed in the $80GeSe_2$-$20Ga_2Se_3$ glass. The peak around 4 Å is due to the Se–Se correlation and corresponds to the space interaction with the second neighbors. Fig. 4(b) shows the neutron structure factors calculated from simulated glass. The first sharp diffraction peak found in $GeSe_2$ glasses [30] now becomes a small shoulder at 1 $Å^{-1}$. The first peak at around 2 $Å^{-1}$ in the total structure factor is dominated by the contribution from Se-Se, while the second peak at around 3.4 $Å^{-1}$ consist of contributions from Se-Se, Ge-Se and Ga-Se.

Table 1 summarizes the bond distances of GeGaSe glass from our AIMD simulations and those from other simulations [26] and experiments [27] for $GeSe_2$. The bond distance for Ge-Se, Ga-Se and Se-Se are 2.50, 2.44 and 2.42 Å, respectively. These bond distances are in general agreement with other simulation work but slightly longer than the experimental value by about 0.1 Å. This could be due to the Generalized Gradient Approximation (GGA) functional with PBE parameterization used in simulations that usually overestimate the lattice parameters and bond

distances. It has been shown that DFT functionals have an effect on the bond distances and simulated glass structures in general [26]. Two different functionals led to bond distances that differ by 0.04 to 0.25 Å for different pairs. The Ge-Ge, Ge-Ga and Ga-Ga distances are 2.48, 3.20 and 3.63 Å, respectively. There are no available experimental data for comparison of these bond distances for this system as deconvolution of the first peak of Fig. 2(b) is challenging due to overlap of contributions of various atom pairs and requires advanced technique such as isotope substitution [27].

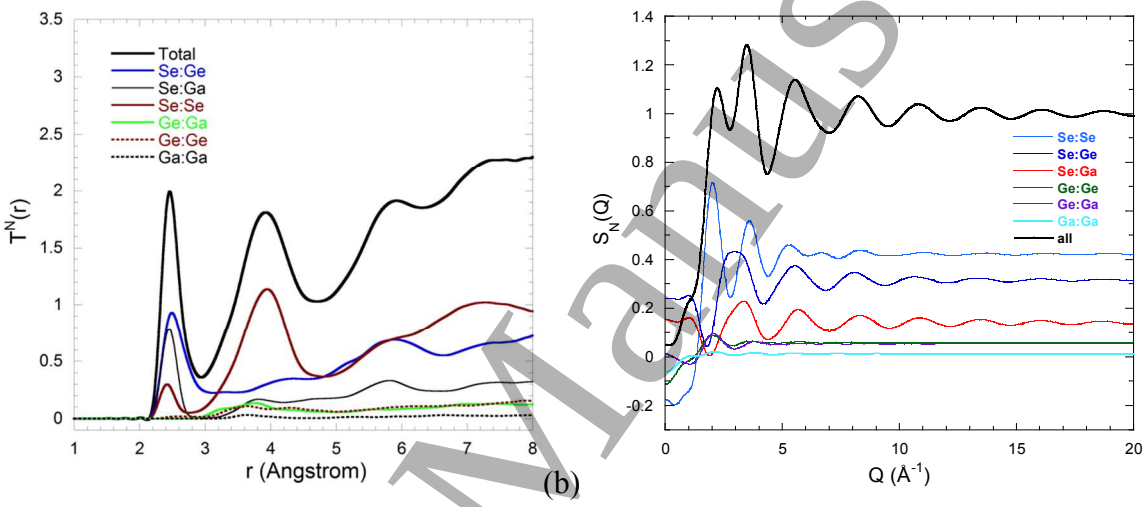

Figure 4: Neutron diffraction total and partial correlation function (a) total and partial structure factors (b) of $80GeSe_2$-$20Ga_2Se_3$ glass from AIMD simulations.

Table 1: Comparison of bond distances (in Å) from AIMD simulations of this work for GeGaSe chalcogenide glasses and other AIMD simulations (for $GeSe_2$) and experimental results (for $GeSe_2$).

Pair	AIMD, this work (PBE)	Ref. 26 (AIMD, BLYP)	Ref. 26 (AIMD, PW91)	Ref. 27 Exp. $GeSe_2$
Ga-Se	2.44	-	-	-
Ge-Se	2.50	2.36	2.41	2.42
Se-Se	2.42	2.38	2.34	2.30
Ge-Ge	2.48	2.45	2.70	2.33
Ga-Ga	3.63	-		
Ga-Ge	3.20	-		

3.4 Local structure around Ge, Ga and Se

The coordination environment around Ge and Ga can be seen in the Ge-Se and Ga-Se pair distribution functions and associated accumulated coordination numbers (Fig. 5). Ga-Se has a sharp and well defined Ga-Se first peak and a clear plateau of cumulated coordination number of four suggesting that Ga is coordinated by four selenium. This is supported by coordination number analysis shown in Fig. 6 and Se-Ga-Se bond angle analysis in Fig. 7, which shows a symmetric peak at around 109° indicating regular [$GeSe_4$] tetrahedron shapes. The suggested preference of four-fold coordinated Ga by Se rather than four-fold coordinated Ge by Se suggested by XPS studies is confirmed by our AIMD simulations [16]. Although Ge is coordinated by less than four Se, its four-fold coordination is partially satisfied by formation of Ge-Ge bonds, again in agreement with the XPS studies [16]. However, no Ge-Ga bonds were observed in simulations as suggested by interpretation of XPS data [16].

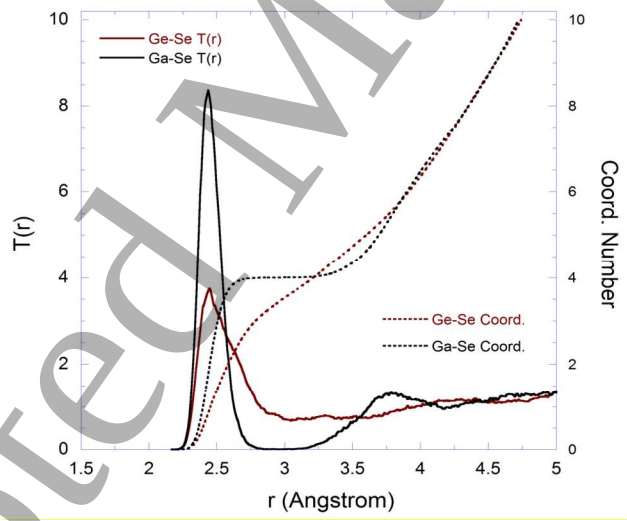

Figure 5: Ge–Se (red) and Ga–Se (black) partial total correlation functions (solid curves). Ge–Se (red) and Ga–Se (black) coordination number curves (dotted curves).

The Ge environment can be understood by the Ge-Se partial pair correlation function (Fig. 5) and bond angle distribution function (Fig. 7). The Ge-Se first peak is broader than the Ga-Se

first peak with a shoulder on the higher r side, suggesting a less well defined first coordination shell. This is also shown in the Se–Ge–Se bond angle distribution (BAD) (Fig. 7 (a) that is much broader than that of Se-Ga-Se with a maximum around 100°, indicating some distortion from the tetrahedral bonding. Se around Ge includes 2, 3, and 4-fold coordination (Fig. 6). This is different from Ga where only 4-fold coordination of Se was observed. This is due to the formation of Ge-Ge homonuclear bonds that distort the [Ge(Ge,Se)$_4$] tetrahedra. Ge-Ge and Ge-Se have similar bond distances (2.48 and 2.50 Å, respectively, Table 1) but the two atoms have different atomic radii (1.25Å for Ge and 1.05Å for Se) hence the tetrahedra are slightly distorted. As compared to 100% 4-fold coordination by Se for Ga, Ge has an average Se coordination number of 3.5. Fig. 6 shows only a half of Ge atoms is 4-fold coordinated by Se, 45% of Ge atoms are 3-fold coordinated by Se, some 5% of 2-fold coordinated by Se. Ge-Ge homonuclear bonds were observed the preservation of 4-fold coordination for Ge atoms but some Ge atoms remain three-fold coordinated by Se (see snapshot of representative environment of Ge and Ga in Fig. 6 (b)).

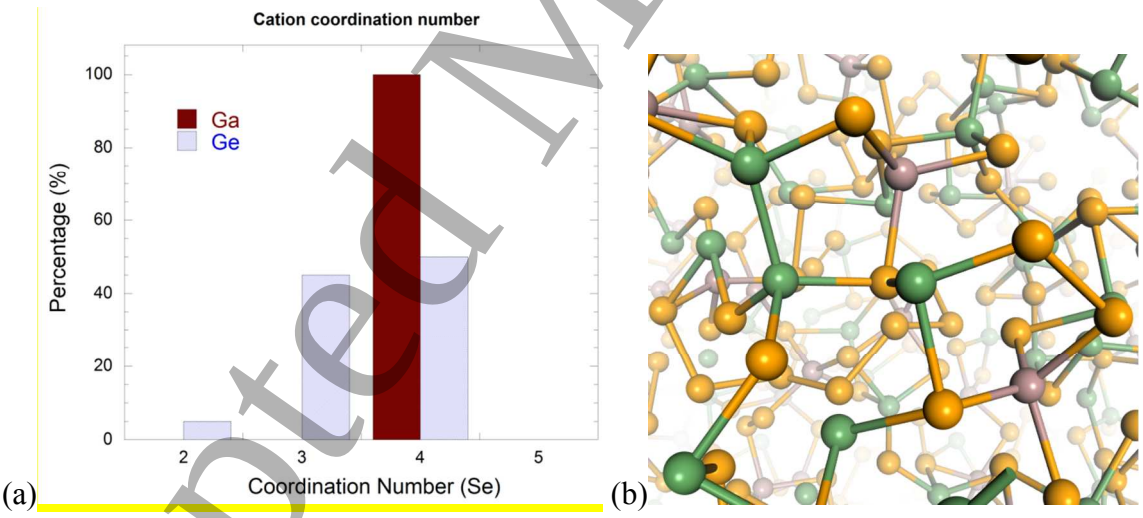

Figure 6: (a) Coordination number distributions of selenium around Ga and Ge atoms in the 80GeSe$_2$-20Ga$_2$Se$_3$ glass. Cutoffs used are 3.1 Å for Ge-Se and 2.8 for Ga-Se. (b) snapshot of structure showing Ge and Ga coordination environments. (yellow balls: Se; green balls: Ge; purple balls: Ga)

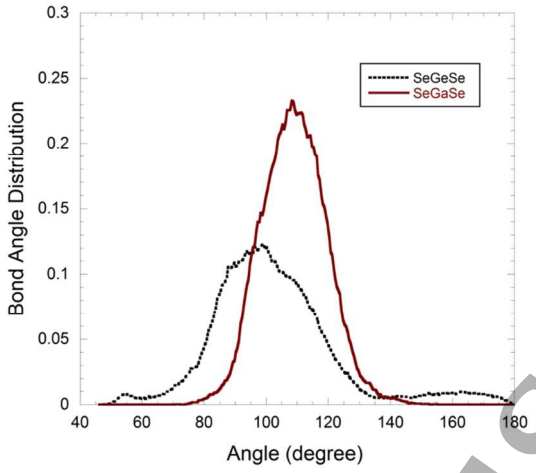

Figure 7: Bond angle distributions (BADs) of Se–Ge–Se (black) and Se–Ga–Se (red). Cutoffs used are 2.50 Å for Ge–Se and 2.44 Å for Ga–Se.

The environment around Se is more complicated. Se atoms are mainly bonded to Ga or Ge to form $GaSe_4$ tetrahedra or $GeSe_x$ polyhedral. There is a higher preference of Se to coordinate around Ga than Ge, as indicated earlier (Fig. 6) that all Ga are four-fold coordinated by Se but Ge are coordinated by both Se and Ge. This can be due to higher ionicity of Ga atoms and this is supported by higher positive charge on Ga than Ge from population analysis (section 3.6). There are also a fraction of Se that forms Se-Se chains with different lengths. The Se-Se bond distance is around 2.42 Å. Selenium chains with length ranging from 2 to 7 selenium atoms were observed in the AIMD generated structures. This kind of Se-Se segregation led to a Se deficient Ge/Ga networks. As a result, other mechanism such as Ge-Ge homonuclear bonds or Se triclusters are formed to satisfy the 4-fold coordination of these Ge and Ga atoms.

3.5 [$GeSe_x$] and [$GaSe_4$] polyhedra connection and Se tricluster

Polyhedron connection analysis was performed for [$GeSe_x$] and [$GaSe_4$]. It was found that [$GaSe_4$]-[$GaSe_4$] tetrahedra connect by corner-sharing Se atoms, while for [$GaSe_4$]-[$GeSe_x$] polyhedra there exist around 80% corner-sharing and 20% edge-sharing. The connections between [$GeSe_x$]-[$GeSe_x$] is more complicated: there are 85% corner-sharing, 10% edge sharing and 5% face-sharing. The formation of a small fraction of high energy and unstable face-sharing [$GeSe_x$] polyhedra could be due to the high cooling rate during glass formation. It is thus

concluded that there exist around 10-15% edge-sharing polyhedrons in the investigated composition but they are mainly between [$GeSe_x$]-[$GeSe_x$] and [$GaSe_4$]-[$GeSe_x$] linkages.

Additionally, the cation environment around Se is analyzed and are summarized in Fig. 8. There are 21% of Se bonded to only 1 cation, among those 35% are Ga atoms and 65% are Ge atoms. Around 36% selenium atoms are bridging selenium, or selenium bond to two cations, among those 62% are bond to 1 Ga and 1 Ge, 10% bond to 2 Ga and 28% bond to 2 Ge. Very importantly, we observed around 36% of selenium atoms that bond to three cations, corresponding to selenium triclusters. Among these triclusters, 60% are 2 Ge and 1 Ga, 15% are 1 Ge and 2 Ga, and the remaining 35% bond to 3 Ge. A very small fraction (<1%) of Se atoms also bond to four Ge atoms. The representative Se triclusters are shown in Fig. 8(b). There are similarity to the oxygen triclusters in aluminosilicate glasses [43]. However, the percentage of oxygen tricluster in aluminosilicate glasses is much lower (only a few percent) than the Se tricluster content in the chalcogenide glasses, which is higher than 35%. This suggests these species are one of the main mechanisms to accommodate selenium deficiency in the glass. The other mechanism is Ge-Ge homonuclear bond that will be discussed in the next section.

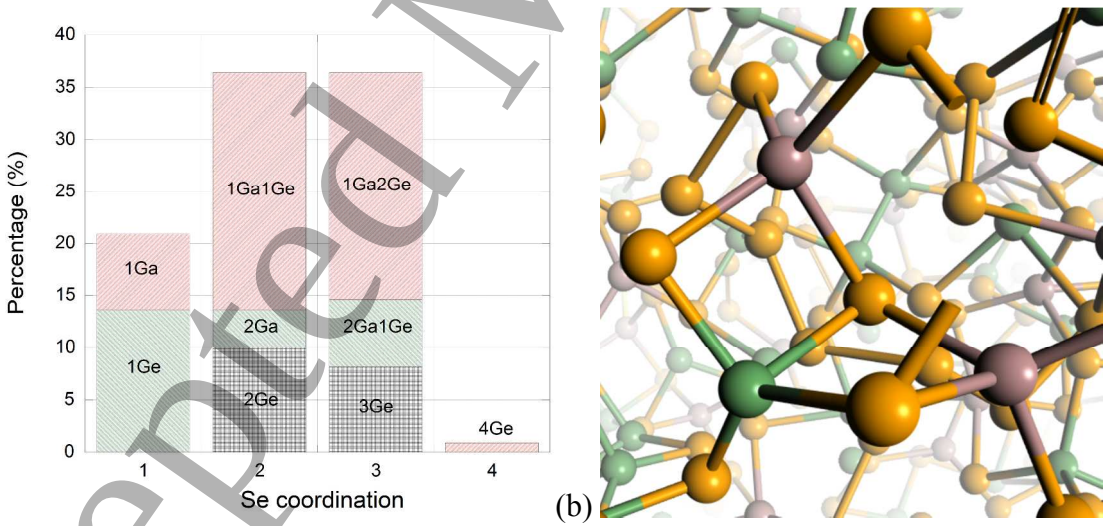

(a) (b)

Fig. 8 (a) Cation coordination distirbution around selenium atoms (b) snapshot of Se tricluster center and edge-sharing $GaSe_4$ and $GeSe_4$ tetrahedra from AIMD simulations for $80GeSe_2$-$20Ga_2Se_3$ glass. (yellow balls: Se; green balls: Ge; purple balls: Ga).

The homonuclear bond formation around Ge and Ga can be analyzed by calculating the cation–cation pair distribution functions as shown in Fig. 9 (a). The Ge-Ga and Ga-Ga first peaks are located at 3.2 and 3.5 Å, respectively, much larger than the sum of their atomic radii (2.6Å for Ga-Ge and 2.7 Å for Ga-Ga) suggesting no direct bond formation between them. This result suggests the assumption of Ga-Ge bond formation used in the RMC simulation based on EXAFS is not a reasonable one [17].

The Ge-Ge pair distribution function has a small peak at 2.48 Å, which is due to Ge-Ge homonuclear bond formation. A snapshot of Ge-Ge homonuclear bond and an adjacent Se tricluster is shown in Fig. 9(b). The Se–Se pair distribution function has a sharp peak at 2.42 Å attests to the existence of homo-nuclear Se–Se bonds. Examination of the structures from AIMD suggested that there exist short chains consisting of 2 to 7 Se atoms (Fig. 3b).

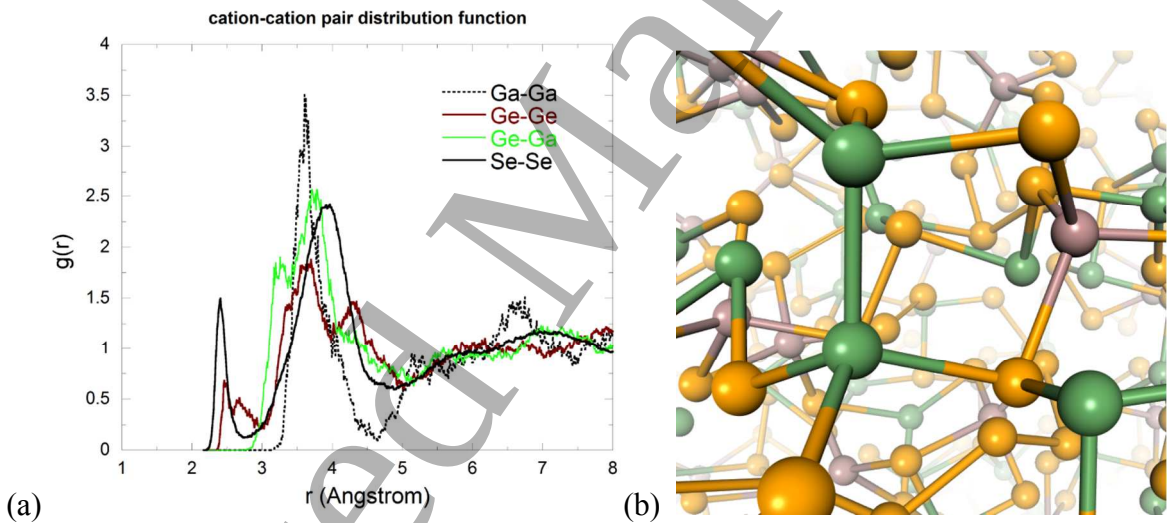

Figure 9 (a) Ga–Ga (dotted black), Ge–Ge (red), Ge–Ga (green) and Se–Se (black) pair distribution functions (b) snapshot showing a Ge-Ge homonuclear bond and an adjacent Se tricluster in the $80GeSe_2$-$20Ga_2Se_3$ glass from AIMD simulations. (yellow balls: Se; green balls: Ge; purple balls: Ga)

3.5 Electronic structure and atomic charges

The electronic structures were calculated from the final glass configurations at 300K after geometrical optimization. Fig. 7 shows the electronic density of states of the simulated glass. The glass structure was fully relaxed before the electronic structure calculations. It is shown that the glass has a very narrow band gap, which is not surprising due to usual underestimation of band gap by conventional DFT [24]. The valence band top is made up of contributions from Se while the conduction band bottom consists contribution from Se and Ge.

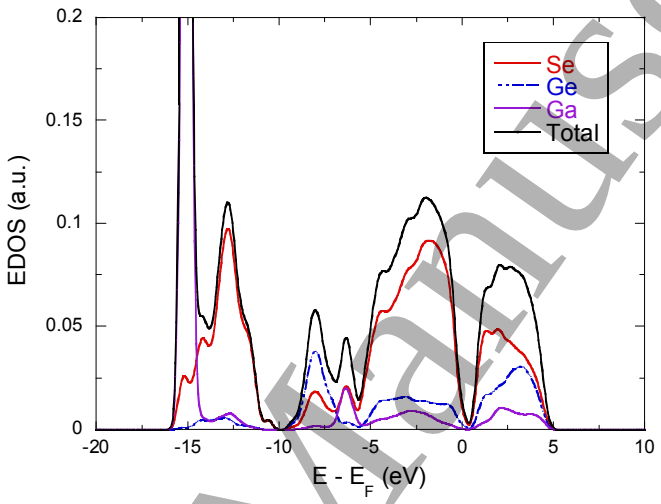

Fig. 10 Total and partial electronic density of states (EDOS) of $80GeSe_2$-$20Ga_2Se_3$ glass.

Population analysis based on the total electron densities from DFT calculations using the Bader method [24, 41] has been performed to obtain atomic charges of all atoms in the glasses. The results show that Se has a fairly large charge variations ranging from -0.674 to 0.064, with an average charge of -0.425 and standard deviation of 0.212. This variation is related to the diverse Se local environments observed in the glasses. Indeed, there exist Se-Se bond (Se chain), Se-Ge (non-bridging), Ge-Se-Ge (bridging), and Se triclusters (one Se bonds to two Ge and one Ga). The charge of Se in each case would be different that lead to large charge variations. The average negative charge indicates that Se mainly plays the anion role in the structure.

The average charge of the cations show much smaller variations. The average charge of Ge is 0.700 with a standard deviation of 0.090. The average charge of Ga is 0.938, higher than Ge, indicating more ionic nature. The standard deviation of Ga charge is 0.010, the smallest deviation

of charges among the three elements in the glass although Ga has the lowest total number. This is consistent with our analysis that shows a more uniform local environment around Ga, 100% 4-fold coordination by selenium and without any homo-nuclear bonds. The atomic charge of Ge (0.700) is smaller than Ga (0.938) indicates a more covalent nature of bonding around Ge than Ga. The variation of the Ge charge is also higher due to a small fraction of Ge forms Ge-Ge homo-nuclear bonds. The atomic charge analyses provide a great way to interpret the chemical bonding and local structures around each types of atoms.

4. Conclusions

An *ab initio* molecular dynamics simulation study of the ternary chalcogenide $80GeSe_2$-$20Ga_2Se_3$ glass was performed in combination with neutron diffraction to elucidate the short- and medium-range structure of this glass. The glass structure data from simulations were compared with neutron diffraction data and show reasonable agreement. Taking into account all the results, we come to a few conclusions concerning the short- and medium-range structure of the $80GeSe_2$-$20Ga_2Se_3$ glass. The glass structure of this system is mainly constituted of [$GaSe_4$] tetrahedra and [$GeSe_x$] (x=2-4) polyhedra linked through corner-sharing through bridging selenium atoms. Average Se coordination around Ge is 3.5, while there also exist Ge-Ge homonuclear bonds to makes most of Ge 4-fold coordinated. [$GaSe_4$] units exhibit close to perfect tetrahedral geometry with a Se–Ga–Se bond angle being around 109°. The [$GeSe_4$] tetrahedra, in contrast, are more distorted. These results are in good agreement with earlier NMR and Raman spectroscopy studies. A significant amount of Se-Se bonds were observed that led to the formation of Se chains, which are also manifested in the Se–Se pair distribution function and consistent with experimental Se NMR studies. A small fraction (less than 0.5 per germanium atom) of homo-nuclear Ge–Ge bonds but no Ga–Ga or Ge–Ga bonds were observed in the structure of the $80GeSe_2$-$20Ga_2Se_3$ glass. This was explained by the higher ionicity of Ga than Ge, as shown in the atomic charges from population analysis. Interestingly, Se tricluster, i.e., selenium atoms that bond to three atoms (Ge or Ga) was also observed in non-trivial amount (around 30%). The Ge-Ge homonuclear bonds and the Se tricluster formation thus consist of two mechanisms to ensure 4-fold coordination of both Ge and Ga in the glasses in situations when Se is deficient either due to glass composition or the formation of Se-Se chains. Electronic structure of the simulated glass

was studied from electronic density of states and Bader population analysis. It was found that atomic charges from population analyses provide further insight and interpretation of the observed structural features. These results show that AIMD simulations, when used carefully and complemented with experimental characterizations, can provide detailed structural information and insights on the structural features of chalcogenide glasses.

Acknowledgements

This work has been supported by a research grant allowed by the Science of Matter PhD School (ED SDLM, Université de Rennes 1). Authors would like also to thank Région Bretagne and Umicore IR Glass for their financial support. J.D. acknowledges financial support of US National Science Foundation DMR Ceramics Program (project # 1508001).

References

[1] J.-L. Adam, X. Zhang, Chalcogenide glasses: Preparation, properties and applications, Electronic, Woodhead Publishing, 2014.

[2] B. Bureau, Recent advences in chalcogenide glasses, J. Non. Cryst. Solids. 345-346 (2004) 276–283.

[3] J.A. Savage, S. Nielsen, Chalcogenide glasses transmitting in the infrared between 1 and 20 μ — a state of the art review, Infrared Phys. 5 (1965) 195–204.

[4] V.F. Kokorina, Glasses for infrared optics, Woodhead Publishing Ltd., Cambridge, 1996.

[5] A.R. Hilton, S. Kemp, Chalcogenide Glasses for Infrared Optics, The McGraw-Hill Companies, New York, 2010.

[6] X.-H. Zhang, Y. Guimond, Y. Bellec, Production of complex chalcogenide glass optics by molding for thermal imaging, J. Non. Cryst. Solids. 326-327 (2003) 519–523.

[7] R. Young, N. Formigoni, Grooved optical data storage device including a chalcogenide memory layer, US4719594 A, 1988.

[8] J.J. Mecholsky, Microstructural Investigation of a Chalcogenide Glass Ceramic, Cathol. Univ. Am. - Washington, D.C. (1973).

[9] J.J. Mecholsky, C.T. Moynihan, P.B. Macedo, G.R. Srinivasan, Microstructure and properties of an infra-red transmitting chalcogenide glass-ceramic, J. Mater. Sci. 11 (1976) 1952–1960.

[10] J. Cheng, Properties and structure of the infrared-transmitting arsenic-germanium-selenium-tin glass-ceramic system, Huadong Huagong Xueyuan Xuebao. 3 (1982) 337–351.

[11] J. Cheng, Phase separation and controlled crystallization of non-oxide, J. Non. Cryst. Solids. 80 (1986) 52–68.

[12] S. Zhu, H.-L. Ma, L. Calvez, X.H. Zhang, J. Lucas, J.L. Adam, et al., Optical and mechanical properties of far infrared transmitting glass ceramics, J. Non. Cryst. Solids. 353 (2007) 1298–1301.

[13] L. Calvez, H.-L. Ma, J. Lucas, X.-H. Zhang, Selenium-Based Glasses and Glass Ceramics Transmitting Light from the Visible to the Far-IR, Adv. Mater. 19 (2007) 129–132.

[14] M. Rozé, L. Calvez, Y. Ledemi, M. Allix, G. Matzen, X.-H. Zhang, Optical and Mechanical Properties of Glasses and Glass-Ceramics Based on the Ge-Ga-Se System, J. Am. Ceram. Soc. 91 (2008) 3566–3570.

[15] M. Rozé, L. Calvez, M. Hubert, P. Toupin, B. Bureau, C. Boussard-Plédel, et al., Molded Glass-Ceramics for Infrared Applications, Int. J. Appl. Glas. Sci. 2 (2011) 129–136.

[16] E. Petracovschi, B. Bureau, A. Moreac, C. Roiland, J.-L. Adam, X.-H. Zhang, L. Calvez, Structural study by Raman spectroscopy and 77 Se NMR of GeSe 4 and 80GeSe 2–20Ga 2 Se 3 glasses synthesized by mechanical milling, J. Non-Cryst. Soids, 421(2016) 16-20.

[17] A. W. Mao, B. G. Aitken, R.E. Youngman, D. C. Kaseman, S. Sen, " Structure of Glasses in the Pseudobinary System Ga2Se3–GeSe2: Violation of Chemical Order and 8-N Coordination Rule", J. Phys. Chem. B 117 (2013) 16594-16601.

[18] A. W. Mao, D. C. Kaseman, I. Hung, Z. Gan, B. G. Aitken, S. Sen, Mechanisms of structural accommodation of Se deficiency in binary Ga 2 Se 3–GeSe 2 glasses: Results from 77 Se MATPASS/CPMG NMR spectroscopy, J. Non-Cryst. Solids, 410 (2015) 14-19.

[19] R. Golovchak, L. Calvez, E. Petracovschi, B. Bureau, D. Savytskii, H. Jain, Incorporation of Ga into the structure of Ge-Se glasses, Material Chemitry Physics, 138 (2013) 909-916.

[20] I. Pethes, R. Chahal, V. Nazabal, C. Prestipino, A. Trapananti, C. Pantalei, B. Beuneu, B. Bureau, P. Jovari, Short range order in Ge-Ga-Se glasses, J. Alloys and Compounds, 541 (2015) 578-584.

[21] J. C. Mauro, A. K. Varshneya, Model interaction potentials for selenium from ab initio molecular simulations, Phys. Rev. B, 71 (2005) 214105.

[22] P. Vashishta, R.K. Kalia, I. Ebbsjö, Structural correlations and phonon density of states in GeSe2: A molecular-dynamics study of molten and amorphous states, Phys. Rev. B. 39 (1989) 6034–6047.

[23] M. Boero, A. Bouzid, S. Le Roux, B. Ozdamar, C. Massoborio, First Principles Molecular Dynamic Methods: an overview, pp 33-56 in C. Massobrio, J. Du, P. S. Salmon, M. Bernasconi (eds), "Molecular Dynamics Simulations of Disordered Materials: from Network Glasses to Phase-Change Memory Alloys", Springer, ISBN 978-3-319-15674-3 (2015).

[24] J. Du and L. R. Corrales, "*ab initio* Molecular Dynamics Study of the Structure, Dynamics, and Electronic Properties of Lithium Disilicate Melt and Glass", *J. Chem. Phys.*, **125** 114702 (2006).

[25] M. Benoit, S. Ispas, P. Jund, R. Jullien, Model of silica glass from combined classical and ab initio molecular – dynamics simulations, Eur. Phys. J. B. 13 (2000) 631–636.

[26] M. Micoulaut, R. Vuilleumier, C. Massobrio, Improved modeling of liquid GeSe2: Impact of the exchange-correlation functional, Phys. Rev. B 79 (2009) 214205.

[27] P. S. Salmon, I. Petri, Structure of glassy and liquid GeSe2, J. Phys. Cond. Matter. 15 (2003) S1509.

[28] M. Durandurdu, D. Drabold, Simulation of pressure-induced polyamorphism in a chalcogenide glass GeSe2, Phys. Rev. B. 65 (2002) 104208 (1–8).

[29] M. Kibalchenko, J.R. Yates, C. Massobrio, A. Pasquarello, Structural Composition of First-Neighbor Shells in GeSe2 and GeSe4 Glasses from a First-Principles Analysis of NMR Chemical Shifts, J. Phys. Chem. C. 115 (2011) 7755–7759.

[30] C. Massobrio, A. Pasquarello, R. Car, Short- and intermediate-range structure of liquid $GeSe_2$, Phy. Rev. B 64 114205 (2001).

[31] I. Voleská, J. Akola, P. Jóvári, J. Gutwirth, T. Wágner, T. Vasileiadis, et al., Structure, electronic, and vibrational properties of glassy Ga11Ge11Te78: Experimentally constrained density functional study, Phys. Rev. B. 86 (2012) 094108 (1–9).

[32] J. Akola, R. O. Jones, Structrual phase transitions on the nanoscale: the crucial patterns in the phase-change materials $Ge_2Sb_2Te_5$ and GeTe, Phys. Rev. B 76 (2007) 235201.

[33] J. Hegedüs, S.R. Elliott , Microstructure origin of the fast crystallization ability of Ge-Sb-Te phase change memory materials, Nat. Mater. **7** (2008) 399.

[34] W. Zhang, V. L. Deringer, R. Dronskowski, R. Mazzarello, E. Ma, M. Wuttig, Density Functional theory guided advances in phase-change materials and memories, MRS Bulletin, 40 (2015) 856.

[35] J.P. Perdew, K. Burke, M. Ernzerhof, Generalized Gradient Approximation Made Simple, Phys. Rev. Lett. 77 (1996) 3865–3868.

[36] S. Nosé, Constant Temperature Molecular Dynamics Methods, Prog. Theor. Phys. Suppl. 103 (1991) 1–46.

[37] B. Bureau, J. Troles, M. Le Floch, P. Guénot, F. Smektala, J. Lucas, Germanium selenide glass structures studied by 77Se solid state NMR and mass spectroscopy, J. Non. Cryst. Solids. 319 (2003) 145–153.

[38] B. Bureau, J. Troles, M. Le Floch, F. Smektala, J. Lucas, Medium range order studied in selenide glasses by 77Se NMR, J. Non. Cryst. Solids. 326 (2003) 58–63.

[39] B. Bureau, C. Boussard-Plédel, M. Le Floch, J. Troles, F. Smektala, J. Lucas, Selenium-Tellurium Sequences in Binary Glasses as Depicted by 77Se and 125Te NMR, J. Phys. Chem. B. 109 (2005) 6130–6135.

[40] Cuello G. J., Darpentigny J., Hennet L., Cormier L., Dupont J., Homatter B. and Beuneu B. (2016) 7C2, the new neutron diffractometer for liquids and disordered materials at LLB. *Journal of Physics: Conference Series* **746**, 012020.

[41] G. Henkelman, A. Arnaldsson, and H. Jónsson, A fast and robust algorithm for Bader decomposition of charge density, Comput. Mater. Sci. **36**, (2006) 254-360.

[42] Y. Xiang and J. Du, "Effect of Strontium Substitution on the Structure of 45S5 Bioglasses", Chem. Mater., **23** (2011) 2703-2717.

[43] J. Du, Molecular Dynamics Simulations of the Structure and Properties of Low Silica Yttrium Aluminosilicate Glasses, J. Am. Ceram. Soc., 92 (2009) 87-95.

[45] A. Wright, The comparison of molecular dynamics simulations with diffraction experiments, J. Non-Cryst. Solids, 159 (1993) 264-268.